ACS OMEGA

http://pubs.acs.org/journal/acsodf

Article

Self-Assembling Metallocomplexes of the Amphiphilic 1,4-Diazabicyclo[2.2.2]octane Derivative as a Platform for the Development of Nonplatinum Anticancer Drugs

Lucia Ya. Zakharova, Alexandra D. Voloshina, Marina R. Ibatullina, Elena P. Zhiltsova, Svetlana S. Lukashenko, Darya A. Kuznetsova,* Marianna P. Kutyreva, Anastasiia S. Sapunova, Anna A. Kufelkina, Natalia V. Kulik, Olga Kataeva, Kamil A. Ivshin, Aidar T. Gubaidullin, Vadim V. Salnikov, Irek R. Nizameev, Marsil K. Kadirov, and Oleg G. Sinyashin

Cite This: *ACS Omega* 2022, 7, 3073−3082

Read Online

ACCESS | Metrics & More | Article Recommendations | Supporting Information

ABSTRACT: New 1-cetyl-4-aza-1-azoniabicyclo[2.2.2]octane bromide complexes with copper(II) bromide and lanthanum(III) nitrate were characterized using dynamic light scattering and transmission electron microscopy, with self-assembly and the morphological behavior elucidated. For the lanthanum(III) nitrate complex, the 3D crystal structure was characterized using X-ray diffractometry. These metallosurfactants were tested as antitumor agents, and a high cytotoxic effect comparable with doxorubicin was revealed against the M-HeLa and A-549 cell lines. Both complexes were 2 times more active toward the MCF-7 cell line than the breast cancer drug tamoxifen. The cytotoxic mechanism of complexes is assumed to be related to the induction of apoptosis through the mitochondrial pathway.

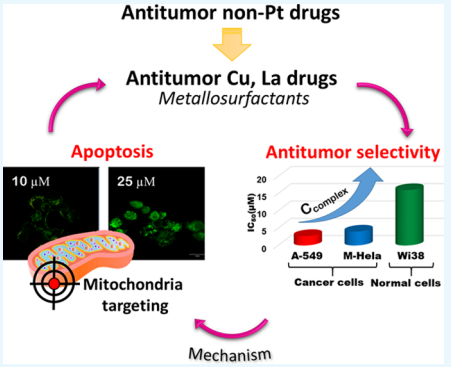

INTRODUCTION

Amphiphilic compounds provide a versatile platform for the development of polyfunctional nanosystems that find wide application in modern nanotechnologies.[1−6] This is due to their ability to form nanosized aggregates in solutions, which can bind a variety of active molecules, thereby modifying their stability and functionality. This is of particular interest for the fabrication of drug and gene nanocarriers. The introduction of functional substituents (including metals) into amphiphilic compounds leads to the appearance of new surfactants with properties potentially useful for biomedicine. According to the literature data, the development of supramolecular systems including liposomes based on surfactants chelated to paramagnetic or radioactive ions Gd(III), ^{64}Cu(II), and ^{111}In(III) as tumor-specific magnetic resonance and single-photon emission tomography contrast agents is of urgent interest.[7−11] At the same time, supramolecular architectures are used to enhance the relaxation of agents.[9,12,13] The ruthenium(II) metallocomplexes based on surfactants with chelating aromatic head groups are fluorescent due to their rich redox/photophysical properties.[14] This opens up a good prospect of using metallosurfactants as fluorescent labels.

The biomedical aspect of the use of metallosurfactants is also associated with an increase in the antimicrobial activity of amphiphiles upon their complexation with metals.[15−22] In this case, surfactants of both anionic and cationic nature serve as ligands.[15−22] Typically, long-chain linear or heterocyclic amines (en, triene, bipyridine, and phenanthroline), amides, and quaternary ammonium salts containing an ester fragment are used as cationic ligands,[16−22] with Co(III), Co(II), Cu(II), Sn(II), Ni(II), La(III), Ru(II), and so forth serving as the metal centers.

One of the actual problems of modern pharmacology is the difficulty in treatment and prevention of oncological diseases unresponsive to various drugs. As a result, it is necessary to search for new safe chemical compounds that will become a drug candidate. It is known that organometallic compounds are widely used in oncological practice.[23,24] Moreover, varying the structure of these compounds (metal type and ligand structure) allows us to search for the most effective drugs and reduce negative side effects.[23−25] The analogues of cisplatin of the second and third generation can serve as a vivid example of varying the structure of ligands.[23] The nonplatinum metals in the complexes of iron, cobalt, copper,

Received: November 16, 2021
Accepted: January 4, 2022
Published: January 14, 2022

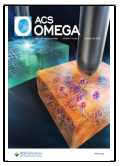

https://doi.org/10.1021/acsomega.1c06465
ACS Omega 2022, 7, 3073−3082

molybdenum, ruthenium, tin, lanthanum, osmium, gold, silver, and so forth are used in oncological pharmacy.[23,25] There are currently a number of nanocarriers including macromolecular structures such as cyclodextrins, dendrimers, liposomes, mesoporous materials, carbon nanotubes, polymer structures, micellar aggregates, and so forth that can be used for the functionalization of metallosurfactants with the goal of targeted drug delivery and protecting them from *in vivo* degradation.[23] At the same time, metallodrugs can be transformed into nanostructures by means of hydrogen bonds, covalent bonds, and hydrophobic and electrostatic interactions. These types of bonds also facilitate the release of the metallocomplex at the desired site.[23] Metal-containing surfactants are attractive in the field of chemotherapy due to their composition and specific properties.[26−29] The increased interest in these compounds is associated with their subsequent use in therapeutic, instrumental, and diagnostic purposes.

The anticancer activity of micelle-forming complexes based on various metals and ligands has been investigated in a number of publications.[26−28,30−33] For these metallosurfactants, literature data are available on the significant role of structural factors (ligand composition, hydrophobicity, and nature of the metal) responsible for the anticancer activity of the complexes. Thus, for the human cervical cancer cell line (M-HeLa), the inhibitory concentration (IC_{50}) for the double-chain surfactant−ruthenium(II) complexes is lower than that for the single-chain complexes.[30]

The objects of our study were new metallosurfactants based on a monoalkylated (cetyl) derivative of 1,4-diazabicyclo[2.2.2]octane (1-cetyl-4-aza-1-azoniabicyclo[2.2.2]octane bromide, $D_{16}Br$) (Figure 1), as

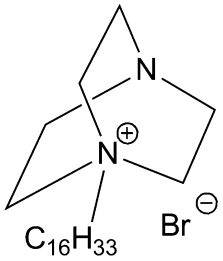

Figure 1. Structural formula of $D_{16}Br$.

well as Cu(II) bromide (**1**) and La(III) nitrate (**2**) composition surfactant: metal = 1:1 ($[Cu(D_{16})Br_3]$) and 2:1 ($[La(D_{16})_2Br_2(NO_3)_3]$), respectively. Previous tensiometric, conductometric, and fluorimetric studies showed that these metal complexes were micelle-forming surfactants. Moreover, their aggregation ability was higher than that of the $D_{16}Br$ ligand and conventional surfactants with the head group of acyclic and monocyclic types (cetyltrimethylammonium bromide and cetylpyridinium bromide).[22,34,35] In addition, the spectrophotometric method showed that supramolecular systems based on metallocomplexes exhibit high solubilization activity with respect to the hydrophobic agent Orange OT dye,[30,31] as well as poorly soluble drugs quercetin and furadonin.[36,37] This allows us to achieve a significant increase in the content of drugs in an aqueous medium (up to 1−2 orders of magnitude) and thereby increase their bioavailability. In addition, a biologically important property of the studied metallosurfactants is their ability to complex with biomolecules (oligonucleotide),[35] as well as the manifestation of antimicrobial and antifungal activity.[21,22] A wide range of functional applications of metallosurfactants require a deeper study of their structural and physicochemical features, as well as functional activity. We established the structure of the lanthanum complex crystal, the size of complex aggregates in solution, and the type of supramolecular structures of both complexes formed in the aqueous medium using X-ray diffractometry (XRD), dynamic light scattering (DLS), and transmission electron microscopy (TEM) methods, respectively. The biological activity of the complexes was studied. These metallosurfactants were tested also as anticancer agents.

RESULTS AND DISCUSSION

Determination of the Spatial Structure of the La(III) Complex Crystals. The crystal structure of the La(III) complex was determined by X-ray single-crystal diffraction. The La ion in the crystal is coordinated by five nitro groups and one water molecule. The asymmetric part of the unit cell (Figure 2) also contains three D_{16} cations and one bromine ion, the latter being disordered over three positions, all near the D_{16} head groups.

Additionally, seven D_{16} molecules oriented by the head groups to the coordination center complete the second coordination sphere and form the complex crystal packing (Figure 3). This arrangement results in the breakage of the trans-conformation of the alkyl chains which change their direction around the 6th−7th carbon atoms starting from the quaternized nitrogen atom. The crystal has a structure composed of hydrophilic and lipophilic layers (see a fragment of the crystal packing of the complex, Figure S1).

Single-Crystal X-ray Investigations of the Structure of the $D_{16}Br$ Ligand. In addition to the complex described above, we obtained the crystals of pure $D_{16}Br$ and their structure was also studied by the single-crystal X-ray diffraction method. According to the data obtained, this compound forms crystals with solvent water molecules. There are two pairs of D_{16}^+ and Br^- ions and one water molecule in the asymmetric part of the monoclinic unit cell (Figure 4). $D_{16}Br$ molecules have a fully elongated linear alkyl part, which, however, is characteristic of most crystallizing molecules with extended hydrocarbon fragments. The C−N bond lengths in the diazabicyclo[2.2.2]octane fragments of both independent molecules have close values and range from 1.441 to 1.510 Å. As can be seen from the shape and size of the ellipsoids of the thermal vibrations of atoms, $D_{16}Br$ molecules do not experience noticeable vibrations or disordering in the crystal.

The supramolecular structure in the crystals of $D_{16}Br$ monohydrate is determined by two factors: the strict localization, in accordance with the previously described rules,[38,39] the hydrophilic and hydrophobic fragments of the molecules in the crystal, and the implementation of many hydrogen bonds C−H···O, CH···Br, OH···N, and CH···N types. Together, these two factors lead to the formation of two-dimensional bilayer supramolecular structures in the crystal (X-ray crystallographic data in Figure S2) located in the crystallographic plane 0*ab*. The inner hydrophilic part of these bilayers is stabilized by numerous intermolecular interactions involving solvate water molecules.

Parallel stacking of such 2D-structures along the crystallographic direction 0*c* is carried out in such a way that only van der Waals interactions are observed between alkyl chains (presented in Figure S2). With such mutual packing of the molecules in the crystal, there are practically no voids

https://doi.org/10.1021/acsomega.1c06465
ACS Omega 2022, 7, 3073−3082

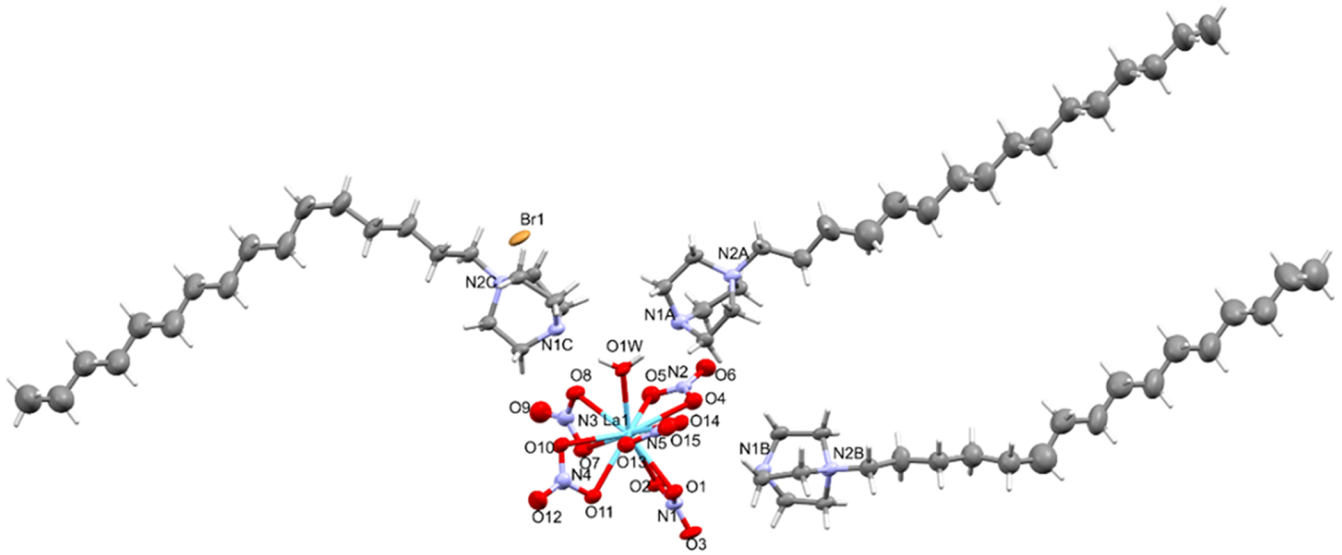

Figure 2. Asymmetric part of the unit cell and La coordination in $D_{16}Br$ with the lanthanum(III) nitrate complex crystal.

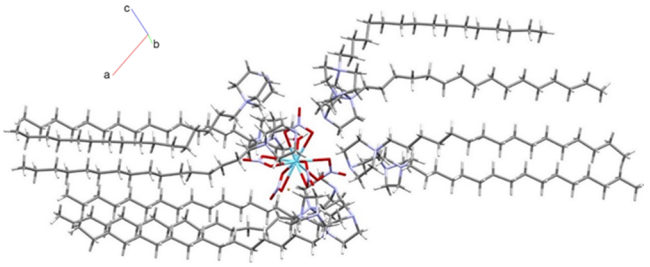

Figure 3. Fragment of the crystal packing of $D_{16}Br$ with the lanthanum(III) nitrate complex showing the $[La(NO_3)_5H_2O]^{2-}$ anion coordination sphere.

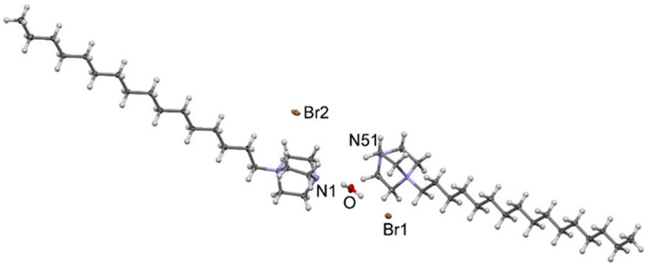

Figure 4. ORTEP view of $D_{16}Br$ in the crystal. Nonhydrogen atoms are represented by probability ellipsoids of thermal vibrations (p = 50%), hydrogen atoms—by spheres of arbitrary radii.

potentially accessible for the solvent, but the packing of the molecules is not dense. The calculated packing index of the molecules, equal to 0.696, approaches the medium of the range characteristic of the crystals of organic compounds (0.65–0.75).[40]

It is interesting to note that this compound crystallizes in the Sohncke space group $P2_1$, although it does not have a chiral center in its composition. Apparently, the manifestation of chirality for the crystals of this compound is related to the nature of the packing of molecules in the crystal, since, as can be seen in Figure S2b, two independent molecules form their own layers in the crystal, consisting only of this molecule. Obviously, in an enantiomeric crystal, the same layers will have the opposite position.

$D_{16}Br$ with the La(III) complex was also characterized by powder X-ray diffraction. In addition to this sample, X-ray diffractograms were also obtained for the starting $D_{16}Br$ sample, which made it possible to control the purity and stability of the systems. According to the powder diffraction data (Figure S3), the calculated and experimental diffraction patterns for the $D_{16}Br$ sample are generally consistent with each other, which indicates that the $D_{16}Br$ powder sample does not contain other crystalline components and is structurally consistent with the $D_{16}Br$ monohydrate crystals. The powder sample of complex **2** is characterized by the presence of some additional diffraction lines. An analysis of the data supports the presence of unreacted residues of crystalline $D_{16}Br$ in the sample complex. In this case, some line shifts in the diffractograms are explained by the difference in the temperature of the powder and single-crystal experiments.

Determination of the Size of Metallocomplex Aggregates by DLS. The method of DLS was used to determine the hydrodynamic diameter of aggregates (D_h, nm) in the aqueous solutions of complex **2** and the composition for comparison containing the ligand–lanthanum nitrate mixture. It has been established that in various concentration ranges of the amphiphile, the formation of supramolecular structures of various types occurs. For metallosurfactant solutions, the aggregates with a size of 70–90 nm are predominantly formed in the critical micelle concentration (CMC) region. There are also a small number of particles (up to 2.5%) of a larger size (310–410 nm). Presumably, these may be the structures of a vesicular or vermiform micellar type. When the CMC is twice exceeded, the small associates (4–6 nm) are mainly formed, which can be attributed to spherical micelles (additional data in Table S1 and Figures S4 and S5). Aggregates of medium diameter are formed in the mixed solutions of $D_{16}Br/La(NO_3)_3{\cdot}6H_2O$ (2:1) in the CMC region as in the complex solutions but with a wider size range of 60–130 nm and up to 1.2% particles with a size of 260–400 nm. In the region of higher concentrations, the formation of spherical micelles with a diameter of 5–7 nm occurs (additional data in Table S1 and Figures S4 and S5). Such size distribution of particles in metal-containing systems is close distribution in the solutions of the ligand itself. According to ref 22, the particles of various types

https://doi.org/10.1021/acsomega.1c06465
ACS Omega 2022, 7, 3073–3082

are formed there. Aggregates of the order of 80 nm and larger particles in the range of 150−300 nm are formed in the CMC region. An increase in the surfactant content also leads to the appearance of small particles (1−9 nm) and a relative increase in their number.

Study of the Structure of Metallosurfactant Aggregates by TEM. The data obtained by TEM are consistent with the results of the DLS on the variety of formed supramolecular structures in solutions. The TEM photographs of the lanthanum complex showed elongated formations with a width of the order of 66−127 nm and a length of usually 169−330 nm and an aspect ratio of structures of the order of 2.5 (in some cases 3.5−5), as well as a rare population of sphere-like particles from <10 to 100 nm in size (Figure 5d,e). The TEM images of the copper complex reflected the formation of individual clearly defined sphere-like particles of 20−50 nm and smaller spherical particles of about 3−7 nm (Figure 5a,b). A combination of small (1−6 nm) and large (120−240 nm) particles of complex **1** (PdI 0.31−0.69 in the CMC region and 0.27−0.47 in the post micellar region) was also observed according to DLS.[22]

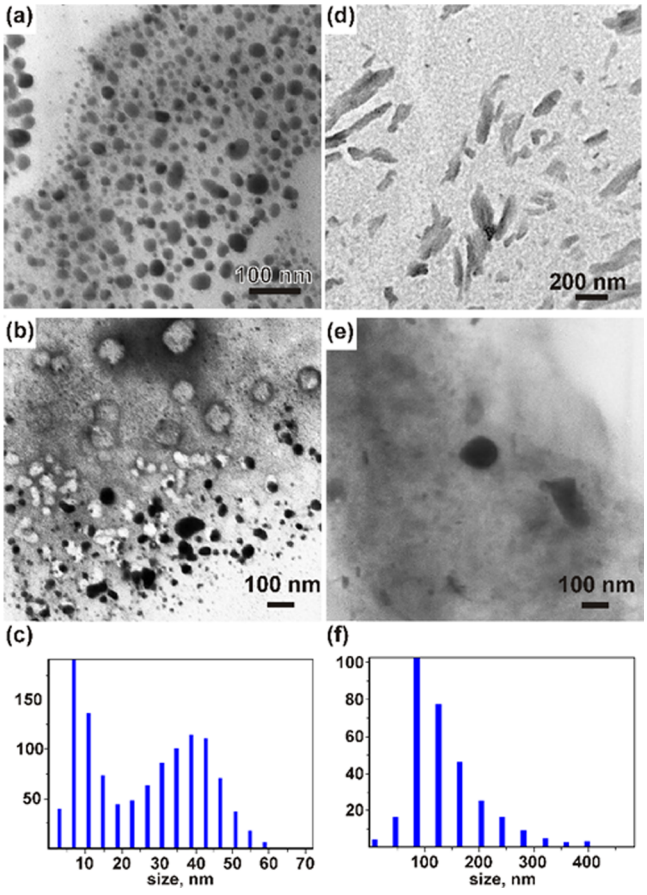

Figure 5. TEM images of copper complex **1** (a,b) and lanthanum complex **2** (d,e) nanoparticles and size distribution curves for complex **1** (c) and **2** (f).

The size distribution curves are shown in Figure 5c,f. For the lanthanum complex, the predominant particle size is about 100 nm, while for the copper complex, the predominant size of the aggregates is in the range of 7 nm.

Cytotoxicity Assay. Taking into account the numerous literature data describing the high biological activity and various fields of application of metallosurfactants, the study of their cytotoxic properties may be of considerable interest. The evaluation of cytotoxic activity *in vitro* is an important stage in the creation of new biologically active compounds. In this regard, we studied the cytotoxic effect of the test compounds **1** and **2** against the lines of normal and human cancer cells at concentrations of 1−100 μM. Table 1 shows the IC_{50} values of the tested compounds. It is seen that both compounds showed high toxicity against all human cancer cell lines. However, compound **1** was found to be more active. Its anticancer activity against the cell lines M-HeLa and A-549 was at the level of the reference drug doxorubicin. Compound **2** showed such high anticancer activity only on the M-HeLa cell line. In relation to the MCF-7 cell line, both compounds were 2 times higher in activity than the reference drug tamoxifen. Importantly, the test compounds were less toxic to normal human cell lines (WI-38) compared to doxorubicin, showing some selectivity toward cancer cells.

Induction of Apoptotic Effects by the Test Compounds. One of the most significant mechanisms of the cytotoxic activity of compounds is the induction of apoptosis, and its assessment is a necessary component of fundamental and applied research in experimental biology. Therefore, using the example of the leading compound **1**, the ability to induce apoptosis in the human cancer cell line M-HeLa was studied. Figures 6 and 7 show that after 24 h of treatment with compound **1**, apoptotic effects were observed in the cells, most pronounced in the stage of early apoptosis. It can be seen that at a concentration of 10 μM, similar to 2 × IC_{50}, compound **1** caused early and late apoptosis in 1.7% and 2.3% of M-HeLa cells, respectively, and with an accretion in the concentration of the test compound to 25 μM, the number of cells in the early apoptosis increased by about 5 times. The results obtained indicate that the mechanism of the cytotoxic action of compound **1** in M-HeLa cells may be due to the apoptotic pathway.

Effects on the Mitochondrial Membrane Potential ($\Delta\psi_m$). There are two main pathways through which apoptotic

Table 1. Cytotoxic Effects of Compounds 1 and 2 on the Cancer and Normal Human Cell Lines[a]

	IC_{50} (μM)				
	cancer line			normal line	
compounds	M-Hela	MCF-7	A549	Chang liver	Wi-38
1	4.0 ± 0.3	14 ± 1.2	2.7 ± 0.2	6.0 ± 0.3	16 ± 0.9
2	4.1 ± 0.3[b]	13 ± 1.1	14 ± 1.3	5.0 ± 0.4[b]	5.0 ± 0.3
doxorubicin	3.0 ± 0.1	3.0 ± 0.2	3.0 ± 0.1	3.0 ± 0.1	1.3 ± 0.1
tamoxifen	28 ± 2.5	25 ± 2.2		42.1 ± 3.5	46.2 ± 3.5

[a]The experiments were repeated three times. [b]Data from ref 41.

https://doi.org/10.1021/acsomega.1c06465
ACS Omega 2022, 7, 3073−3082

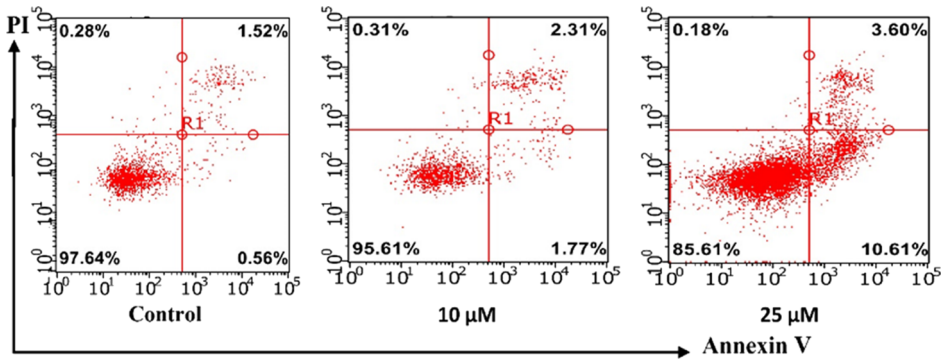

Figure 6. Apoptotic effects of compound **1** on M-HeLa cells.

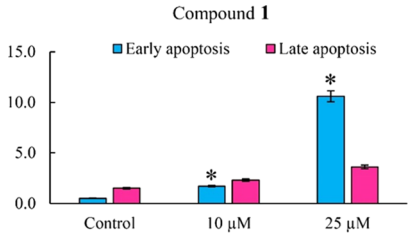

Figure 7. Histogram for the number of cells (% of total) in the early and late stages of apoptosis for the control and experimental groups. The values are presented as the mean ± SD (n = 3); (*) $P < 0.01$ compared to control.

signals are transmitted in the form of cellular regulators such as hormones, antigens, monoclonal antibodies, and other molecules. This is the mitochondrial (or internal) pathway, as well as through special transmembrane proteins—the so-called death receptors (external pathway). In both cases, in order to trigger apoptosis, special initiator apoptotic complexes must be formed. The mitochondrial pathway is initiated as a result of intense exposure of the cell to a number of damaging factors, including chemical agents.[42]

The ability of the studied compounds to induce apoptosis proceeding along the mitochondrial pathway, causing a decrease in the mitochondrial membrane potential ($\Delta\psi_m$) in M-HeLa culture cells, was evaluated using the example of compound **1**. Studies were performed by flow cytometry methods using the JC-10 reagent. In normal cells with a high mitochondrial membrane potential, the dye JC-10 forms aggregates (J-aggregate) near the mitochondrial membranes. When the membrane potential falls due to the stimulation of apoptosis, JC-10 is evenly distributed in the cell as a monomer (J-monomer). JC-10 aggregates in normal cells have red fluorescence, while JC-10 monomers are green. The ratio between orange-red and green fluorescence can be used to judge the onset of apoptosis.

Figure 8a shows that in control samples with a high mitochondrial membrane potential, red to orange luminosity is dominant. A similar staining was observed in the tested samples after exposure to a lower concentration (10 μM), which indicates a partial preservation of the mitochondrial membrane potential and the stage of early apoptosis in M-HeLa cells. In experimental samples treated with the test compound at a concentration of 25 μM, green fluorescence prevailed, demonstrating the process of depolarization of the mitochondrial membrane and the stage of late apoptosis. The decrease in $\Delta\psi_m$ was also confirmed by flow cytometry analysis (Figure 8b). The intensity of red fluorescence decreased depending on the concentration of the test compound.

The obtained results testify that the mechanism of the cytotoxic action of the tested compounds may be due to the induction of apoptosis, proceeding along the mitochondrial pathway.

CONCLUSIONS

Thus, new amphiphilic complexes of monoquaternized bicyclic diamine 1,4-diazabicyclo[2.2.2]octane with transition metals [copper(II) and lanthanum(III) ions] were obtained and characterized by physicochemical methods (XRD, DLS, and TEM). The 3D crystal structure of metallosurfactants and their ability to self-associate in solution were described. A variety of morphological forms of amphiphilic complexes were established. It was shown that along with high aggregation, adsorption, solubilization properties, and antimicrobial activity, the studied complexes exhibited a cytotoxic effect. The anticancer activity of metallosurfactants to M-HeLa, A-549, and MCF-7 cell lines was at the level or 2 times higher than the test drugs doxorubicin and tamoxifen. Moreover, the studied amphiphiles were less toxic in relation to normal human cell lines compared with doxorubicin. Using flow cytometry, laser confocal microscopy, and fluorimetry on the Cytell Cell Imaging system, it was shown that metallocomplexes actively induced apoptosis in M-HeLa cells and caused a significant decrease in the mitochondrial membrane potential at the tested concentrations. This suggests that the mechanism of the cytotoxic action of the tested compounds may be due to the induction of apoptosis, proceeding along the mitochondrial pathway. According to the literature,[23,24] it can be noted that this study also lays the foundation for future work on the development of new nonplatinum anticancer drugs with increased selectivity for cancer cells.

EXPERIMENTAL SECTION

Materials. $D_{16}Br$ (ligand) was prepared by the quaternization of 1,4-diazabicyclo[2.2.2]octane (97%, Acros Organics, USA) with cetyl bromide (98%, Alfa Aesar, Germany) by the procedure.[43] Complexes **1** and **2** were synthesized in methanol and acetone by the procedure.[34,36] The compositions of the products were confirmed by IR and ^{1}H NMR spectroscopy, elemental analysis, and for the crystals of metallocomplex **1** by single-crystal XRD (in Figure S6).[31] $La(NO_3)_3{\cdot}6H_2O$ (98%) (Acros-Organics, USA) was used as received. Water for preparing the solutions was purified using a Millipore Direct-Q 5 UV system.

https://doi.org/10.1021/acsomega.1c06465
ACS Omega 2022, 7, 3073−3082

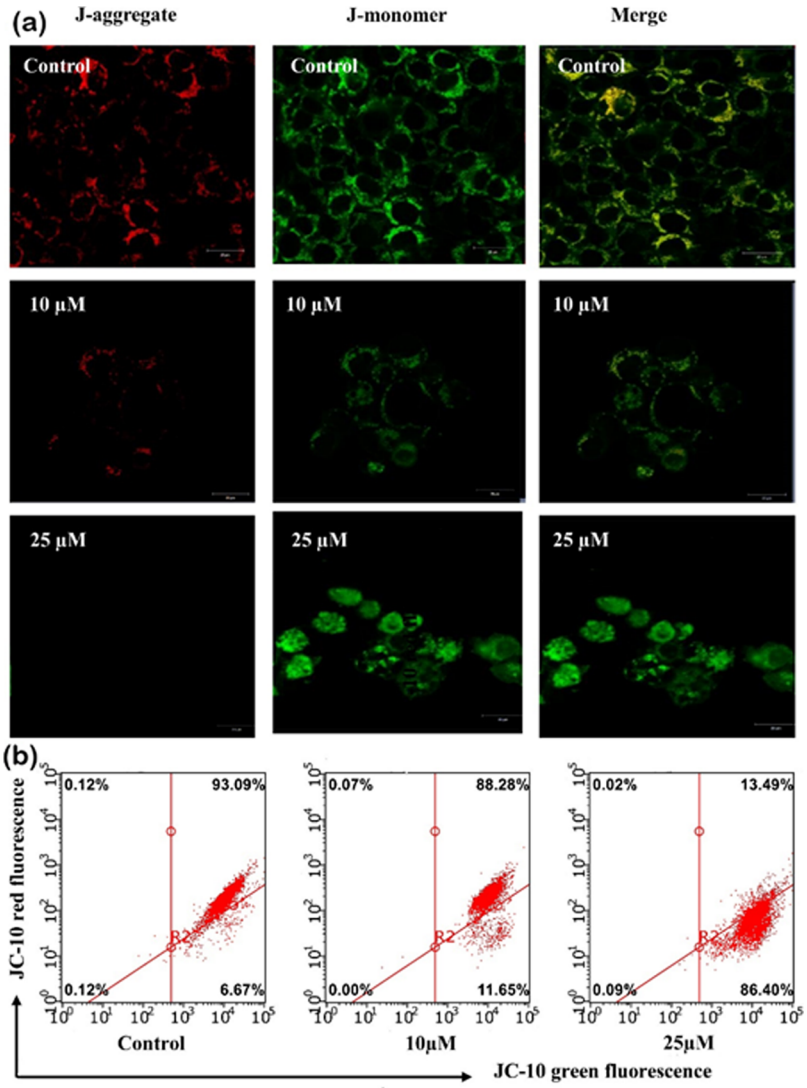

Figure 8. Effects on $\Delta\psi_m$ in M-HeLa cells that were treated with compound **1** at the indicated concentrations for 24 h and then analyzed by confocal laser scanning microscopy and flow cytometry after JC-10 staining. (a) Confocal laser scanning microscopy images of M-HeLa cells treated with compound **1**. (b) Flow cytometry analysis of M-HeLa cells treated with **1**.

Dynamic Light Scattering. The sizes of the aggregates were determined by DLS measurements using a Malvern Zetasizer Nano nanoparticle characterization system (UK). A He−Ne gas laser with 4 mW power and 633 nm wavelength was used as a source of laser radiation. All measurements were performed at 173° light scattering angle. The effective hydrodynamic radius was calculated according to the Einstein−Stokes equation. The diffusion coefficient was measured three times for each sample. The average error of measurements did not exceed 4%.

Transmission Electron Microscopy. TEM was performed on a Hitachi HT7700 (tungsten filament, HV = 80 kV). The samples were deposited on a 300 mesh copper grid with a continuous carbon-formvar support film.

X-ray Crystallography. A Bruker Kappa Apex II CCD diffractometer was used to collect single-crystal data for $D_{16}Br$ and its complex with lanthanum(III) nitrate (ω- and φ-scan modes, graphite monochromated Mo K_α [λ = 0.71073 Å) radiation, 150(2) K]. The data were corrected for the absorption effect using the SADABS program.[44] The features of the structure decoding process are given in the Supporting Information.

Crystal data for $D_{16}Br$: formula $2(C_{22}H_{45}N_2)^+$, $2(Br)^-$, H_2O, M = 853.03 g/mol, monoclinic, space group $P2_1$ (no. 4), Z = 2, a = 5.82828(16) Å, b = 6.9310(19) Å, c = 56.791(15) Å, β = 92.934(3)°, V = 2291(1) Å^3, ρ_{calc} = 1.237 g cm^{-3}, μ = 1.805 mm^{-1}, 19,689 reflections collected ($-7 \le h \le 7$, $-9 \le k \le 8$, $-74 \le l \le 74$), θ range = 2.154 to 27.999°, 10,132 independent (R_{int} = 0.0648) and 7467 observed reflections [$I \ge 2\sigma(I)$], 468 refined parameters, R = 0.0549, wR^2 = 0.0891, goodness of fit S = 0.943, and maximum (minimum) residual electron density 0.691 (−0.611) e Å^{-3}.

Crystal data for the complex of $D_{16}Br$ with lanthanum(III) nitrate: formula $[La(NO_3)_5 \cdot H_2O]^{2-} \cdot 3D_{16}^+ \cdot Br^-$ ($C_{66}H_{137}BrLaN_{11}O_{16}$), M = 1559.68 g/mol, monoclinic, space group $P2_1/c$ (no. 14), Z = 4, a = 29.689(5) Å, b = 14.194(2) Å, c = 20.253(3) Å, β = 108.716(2)°, V = 8083(2) Å^3, ρ_{calc} = 1.282 g cm^{-3}, μ = 1.088 mm^{-1}, 165,523 reflections collected ($-39 \le h \le 39$, $-19 \le k \le 19$, $-27 \le l \le 27$), θ range = 1.607° to 28.569°, 20,511 independent (R_{int} = 0.0800) and 13,962 observed reflections [$I \ge 2\sigma(I)$], 910 refined

https://doi.org/10.1021/acsomega.1c06465
ACS Omega 2022, 7, 3073−3082

parameters, R = 0.0471, wR^2 = 0.1201, and maximum residual electron density 1.047 (−0.920) e Å^{-3}. Bromine ion and alkyl groups are disordered; the maximum residual density is located near the Br atom.

X-ray Powder Diffraction Experiments. Powder X-ray diffraction measurements were performed on a Bruker D8 ADVANCE diffractometer equipped with Vario attachment and Vantec linear PSD using Cu radiation (40 kV, 40 mA) monochromated by a curved Johansson monochromator (λ Cu $K_{\alpha 1}$ 1.5406 Å). Room-temperature data were collected in the reflection mode. The samples were loaded on a standard zero-diffraction silicon plate, which was kept spinning (15 rpm) throughout the data collection. The samples were preliminarily ground to a homogeneous state and then, without pressing, were applied onto a silicon plate, which reduces background scattering. The patterns were recorded in the 2Θ range between 3 and 70° in 0.008° steps with a step time of 0.1−1.0 s. The processing of the obtained data was performed using EVA software packages.[45]

Biological Study. *Cell Lines.* M-HeLa clone 11 human, epithelioid cervical carcinoma, strain of HeLa, clone of M-HeLa, human breast adenocarcinoma cells (MCF-7), human lung adenocarcinoma (A 549), WI-38 VA-13 cell culture, and subline 2RA (human normal embryonic lung cells) were purchased from the Type Culture Collection of the Institute of Cytology (Russian Academy of Sciences). Human normal liver cells (Chang liver) were purchased from the N. F. Gamaleya Research Center of Epidemiology and Microbiology.

Cytotoxicity Assay. The cytotoxic activity of metallosurfactants against cancer and normal human cell lines was assessed using the Cell Viability Bio application of the Cytell multifunctional cell imaging system (GE Health Care Life Science, Sweden). This system makes it possible to estimate the cell viability from the fluorescence intensity. In the experiments, an intercalating dye 4′,6-diamidine-2-phenylindole (DAPI) was used for the intravital staining of cell nuclei in blue and a high-molecular intercalating dye propidium iodide, which penetrates only dead cells, staining them yellow. As a result, the living cells were colored blue, while the dead cells were colored yellow. DAPI and propidium iodide were purchased from Sigma-Aldrich (Merck). The cells were cultured in a standard Eagle's nutrient medium, produced at the Institute of Poliomyelitis and Viral Encephalitis, Chumakov (PanEko company), with the addition of 10% fetal calf serum and 1% nonessential amino acids. The cells were seeded in a 96-well plate (Eppendorf) in 150 μL of the medium at an amount of 1.5 × 10^4 cells/well and cultured in a CO_2 incubator at 37 °C. After a 24 h incubation, the spent medium was removed and 150 μL of the test compound was added in a pre-established dilution, 150 μL in each well. Dilutions of the compounds were prepared directly in a nutrient medium. To improve the solubility, 5% DMSO was added to the medium, which does not induce cell inhibition at this concentration. Intact cells cultured simultaneously with experimental cells were used as controls.

Cell Viability Bio application was used to calculate the cell viability as a percentage of control. The results of the cytotoxicity assay are presented as the concentration of the test compound that inhibits cell growth by 50% (IC_{50}). Doxorubicin and tamoxifen, purchased from Sigma-Aldrich (Merck), were used as the standard drugs.

Flow Cytometry Assay. *Cell Culture.* M-HeLa cells at 1 × 10^6 cells/well were added to 6-well plates, 2 mL in each well. For the confocal laser scanning microscopy assay, a cover glass was placed at the bottom of each well. After a 24 h incubation, the spent medium was removed and solutions of lead compound **1** were added at concentrations 10 and 25 μM. Then, the samples were incubated for 24 h in a CO_2 incubator at 37 °C.

Cell Apoptosis Analysis. The cells were detached using a mixture of trypsin−Versene (1:3), suspended in phosphate-buffered saline (PBS) and centrifuged at 2000 rpm for 5 min, and then washed twice with ice-cold PBS, followed by resuspension in the binding buffer. Next, the samples were incubated with 5 μL of annexin V-FITC (Sigma-Aldrich, Merck) and 5 μL of propidium iodide for 15 min at room temperature in the dark. Finally, the cells were analyzed by flow cytometry (Guava easyCyte, Merck, USA).

Mitochondrial Membrane Potential. The M-HeLa cells were detached using a mixture of trypsin−Versene (1:3), suspended in PBS and centrifuged at 2000 rpm for 5 min, and then washed twice with ice-cold PBS, followed by resuspension in PBS. Further, the samples were added with 10 μg/mL of the JC-10 Mitochondrial Membrane Potential Assay Kit (Sigma-Aldrich, Merck) and incubated at 37 °C for 10 min. After the cells were rinsed three times and suspended in PBS, JC-10 fluorescence was observed by flow cytometry.

Confocal Laser Scanning Microscopy Assay. The M-HeLa cells grown on cover glasses were treated with lead compound **1** at concentrations of 10 and 25 μM and stained with a fluorescent dye JC 10 in the dark for 15 min. Then, the samples were washed with the buffer provided by the manufacturer as part of the JC-10 Mitochondrial Membrane Potential Assay Kit (Sigma-Aldrich, Merck). Confocal microscopy studies were carried out using a laser confocal microscope LSM 780.

Statistical Analysis. IC_{50} calculation was performed with an internet tool: MLA—"Quest Graph IC_{50} Calculator." AAT Bioquest, Inc., December 17, 2020, https://www.aatbio.com/tools/ic50-calculator.[46] The data in the tables and graphs are given as the mean ± standard error. All assays were performed in triplicate.

■ ASSOCIATED CONTENT

Supporting Information

The Supporting Information is available free of charge at https://pubs.acs.org/doi/10.1021/acsomega.1c06465.

X-ray crystallography of the lanthanum(III) complex and ligand, powder diffraction patterns, and hydrodynamic diameter of the aggregates (PDF)

Crystallographic data of D_{16}Br (CIF)

Crystallographic data of D_{16}Br with lanthanum(III) (CIF)

Accession Codes

CCDC 1965797 and 1976025 contain the supplementary crystallographic data for this paper. These data can be obtained free of charge via www.ccdc.cam.ac.uk/data_request/cif, or by emailing data_request@ccdc.cam.ac.uk, or by contacting The Cambridge Crystallographic Data Centre, 12 Union Road, Cambridge CB2 1EZ, UK; Fax: +44 1223 336033.

■ AUTHOR INFORMATION

Corresponding Author

Darya A. Kuznetsova − *Arbuzov Institute of Organic and Physical Chemistry, FRC Kazan Scientific Center of RAS,*

https://doi.org/10.1021/acsomega.1c06465
ACS Omega 2022, 7, 3073−3082

Kazan 420088, Russia; orcid.org/0000-0002-6981-4868; Email: dashyna111@mail.ru

Authors

Lucia Ya. Zakharova − *Arbuzov Institute of Organic and Physical Chemistry, FRC Kazan Scientific Center of RAS, Kazan 420088, Russia;* orcid.org/0000-0002-2981-445X

Alexandra D. Voloshina − *Arbuzov Institute of Organic and Physical Chemistry, FRC Kazan Scientific Center of RAS, Kazan 420088, Russia*

Marina R. Ibatullina − *A.M. Butlerov Chemistry Institute, Kazan Federal University, Kazan 420008, Russia*

Elena P. Zhiltsova − *Arbuzov Institute of Organic and Physical Chemistry, FRC Kazan Scientific Center of RAS, Kazan 420088, Russia*

Svetlana S. Lukashenko − *Arbuzov Institute of Organic and Physical Chemistry, FRC Kazan Scientific Center of RAS, Kazan 420088, Russia;* orcid.org/0000-0002-6415-1161

Marianna P. Kutyreva − *A.M. Butlerov Chemistry Institute, Kazan Federal University, Kazan 420008, Russia*

Anastasiia S. Sapunova − *Arbuzov Institute of Organic and Physical Chemistry, FRC Kazan Scientific Center of RAS, Kazan 420088, Russia*

Anna A. Kufelkina − *Arbuzov Institute of Organic and Physical Chemistry, FRC Kazan Scientific Center of RAS, Kazan 420088, Russia*

Natalia V. Kulik − *Arbuzov Institute of Organic and Physical Chemistry, FRC Kazan Scientific Center of RAS, Kazan 420088, Russia*

Olga Kataeva − *Arbuzov Institute of Organic and Physical Chemistry, FRC Kazan Scientific Center of RAS, Kazan 420088, Russia;* orcid.org/0000-0002-9763-5947

Kamil A. Ivshin − *A.M. Butlerov Chemistry Institute, Kazan Federal University, Kazan 420008, Russia*

Aidar T. Gubaidullin − *Arbuzov Institute of Organic and Physical Chemistry, FRC Kazan Scientific Center of RAS, Kazan 420088, Russia*

Vadim V. Salnikov − *Kazan Institute of Biochemistry and Biophysics, FRC Kazan Scientific Center of RAS, Kazan 420111, Russia*

Irek R. Nizameev − *Arbuzov Institute of Organic and Physical Chemistry, FRC Kazan Scientific Center of RAS, Kazan 420088, Russia*

Marsil K. Kadirov − *Arbuzov Institute of Organic and Physical Chemistry, FRC Kazan Scientific Center of RAS, Kazan 420088, Russia*

Oleg G. Sinyashin − *Arbuzov Institute of Organic and Physical Chemistry, FRC Kazan Scientific Center of RAS, Kazan 420088, Russia*

Complete contact information is available at: https://pubs.acs.org/10.1021/acsomega.1c06465

Author Contributions

L.Y.Z. and O.G.S. provided the fundamental plans and supervised the chemical part and the whole research project, respectively. A.D.V. carried out the biological assay. M.R.I. and E.P.Z. performed the preparation of all samples for investigations, as well as the study on aggregation using dynamic and electrophoretic light scattering techniques. S.S.L. carried out the synthesis of metallocomplexes. D.A.K. carried out literature review and editing of the manuscript. M.P.K. prepared the part of the manuscript on the structure and composition of the complexes. A.S.S., A.A.K., and N.V.K. accomplished investigations of complexes for anticancer and cytotoxic activity, as well as the ability to induce apoptosis. O.N.K. and K.A.I. performed X-ray crystallography experiments. A.T.G. performed X-ray single crystal ($D_{16}Br$) and powder diffraction experiments. V.V.S., I.R.N., and M.K.K. conducted the study using the electron microscopy technique, including sample preparation, interpretation, and discussion of the results.

Notes

The authors declare no competing financial interest.

■ ACKNOWLEDGMENTS

This work was financially supported by the Russian Science Foundation (project no. 19-73-30012).

■ ABBREVIATIONS

XRD, X-ray diffractometry; DLS, dynamic light scattering; TEM, transmission electron microscopy; $D_{16}Br$, 1-cetyl-4-aza-1-azoniabicyclo[2.2.2]octane bromide; CMC, critical micelle concentration

■ REFERENCES

(1) Gontsarik, M.; Yaghmur, A.; Ren, Q.; Maniura-Weber, K.; Salentinig, S. From Structure to Function: PH-Switchable Antimicrobial Nano-Self-Assemblies. *ACS Appl. Mater. Interfaces* **2019**, *11*, 2821−2829.

(2) Daso, R. E.; Mitchell, S. M.; Lebedenko, C. G.; Heise, R. M.; Banerjee, I. A. Exploring the Interactions of Ionic Liquids with Bio-Organic Amphiphiles Using Computational Approaches. *ACS Omega* **2021**, *6*, 32460−32474.

(3) Zakharova, L.; Mirgorodskaya, A.; Zhiltsova, E.; Kudryavtseva, L.; Konovalov, A. Reactions in Supramolecular Systems. *Molecular Encapsulation: Organic Reactions in Constrained Systems* **2010**, 397−420.

(4) Di Francesco, M.; Celia, C.; Cristiano, M. C.; d'Avanzo, N.; Ruozi, B.; Mircioiu, C.; Cosco, D.; Di Marzio, L.; Fresta, M. Doxorubicin Hydrochloride-Loaded Nonionic Surfactant Vesicles to Treat Metastatic and Non-Metastatic Breast Cancer. *ACS Omega* **2021**, *6*, 2973−2989.

(5) Kuznetsova, D. A.; Gaynanova, G. A.; Vasileva, L. A.; Sibgatullina, G. V.; Samigullin, D. V.; Sapunova, A. S.; Voloshina, A. D.; Galkina, I. V.; Petrov, K. A.; Zakharova, L. Y. Mitochondria-targeted cationic liposomes modified with alkyltriphenylphosphonium bromides loaded with hydrophilic drugs: preparation, cytotoxicity and colocalization assay. *J. Mater. Chem. B* **2019**, *7*, 7351−7362.

(6) Kuznetsova, D. A.; Gabdrakhmanov, D. R.; Lukashenko, S. S.; Voloshina, A. D.; Sapunova, A. S.; Kulik, N. V.; Nizameev, I. R.; Kadirov, M. K.; Kashapov, R. R.; Zakharova, L. Y. Supramolecular systems based on cationic imidazole-containing amphiphiles bearing hydroxyethyl fragment: Aggregation properties and functional activity. *J. Mol. Liq.* **2019**, *289*, 111058.

(7) Chen, Y.; Zhu, Q.; Tian, Y.; Tang, W.; Pan, F.; Xiong, R.; Yuan, Y.; Hu, A. Supramolecular aggregates from polyacrylates and Gd(III)-containing cationic surfactant as high-relaxivity MRI contrast agents. *Polym. Chem.* **2015**, *6*, 1521−1526.

(8) Mitchell, N.; Kalber, T. L.; Cooper, M. S.; Sunassee, K.; Chalker, S. L.; Shaw, K. P.; Ordidge, K. L.; Badar, A.; Janes, S. M.; Blower, P. J.; Lythgoe, M. F.; Hailes, H. C.; Tabor, A. B. Incorporation of paramagnetic, fluorescent and PET/SPECT contrast agents into liposomes for multimodal imaging. *Biomaterials* **2013**, *34*, 1179−1192.

(9) Gong, P.; Chen, Z.; Chen, Y.; Wang, W.; Wang, X.; Hu, A. High-relaxivity MRI contrast agents prepared from miniemulsion polymerization using gadolinium(III)-based metallosurfactants. *Chem. Commun.* **2011**, *47*, 4240−4242.

(10) Vaccaro, M.; Mangiapia, G.; Radulescu, A.; Schillén, K.; D'Errico, G.; Morelli, G.; Paduano, L. Colloidal particles composed of amphiphilic molecules binding gadolinium complexes and peptides as tumor-specific contrast agents in MRI: Physico-chemical characterization. *Soft Matter* **2009**, *5*, 2504−2512.
(11) Hovland, R.; Aasen, A. J.; Klaveness, J. Preparation and in vitro evaluation of GdDOTA-(BOM)4; a novel angiographic MRI contrast agent. *Org. Biomol. Chem.* **2003**, *1*, 1707−1710.
(12) Usselman, R. J.; Qazi, S.; Aggarwal, P.; Eaton, S. S.; Eaton, G. R.; Russek, S.; Douglas, T. Gadolinium-Loaded Viral Capsids as Magnetic Resonance Imaging Contrast Agents. *Appl. Magn. Reson.* **2015**, *46*, 349−355.
(13) Accardo, A.; Tesauro, D.; Aloj, L.; Pedone, C.; Morelli, G. Supramolecular aggregates containing lipophilic Gd(III) complexes as contrast agents in MRI. *Coord. Chem. Rev.* **2009**, *253*, 2193−2213.
(14) Nehru, S.; Veeralakshmi, S.; Arunachalam, S. Synthesis, characterisation and self-assembly behaviour of emissive surfactant-ruthenium(ii) complexes. *New J. Chem.* **2017**, *41*, 13830−13837.
(15) Tawfik, S. M.; Zaky, M. F. Synthesis, Structure Characterization and Biological Activity of Co (II), Cu (II), and Zn (II) Complexes with (Z)-3-((3-hydroxybenzylidene)amino)pyridin-1-ium 4-(dodecan-4-yl)benzenesulfonate Surfactant. *J. Surfactants Deterg.* **2015**, *18*, 863−871.
(16) Kumar, R. S.; Arunachalam, S. Synthesis, micellar properties, DNA binding and antimicrobial studies of some surfactant-cobalt(III) complexes. *Biophys. Chem.* **2008**, *136*, 136−144.
(17) Kumar, R.; Arunachalam, S.; Periasamy, V.; Preethy, C.; Riyasdeen, A.; Akbarsha, M. Surfactant-cobalt(III) complexes: Synthesis, critical micelle concentration (CMC) determination, DNA binding, antimicrobial and cytotoxicity studies. *J. Inorg. Biochem.* **2009**, *103*, 117−127.
(18) I Adawy, A.; A Badr, E. Synthesis and Biological Activity of Some Amide-Based Cationic Surfactant complexes with Co (II) and Cu (II). *IOSR J. Appl. Chem.* **2014**, *7*, 09−19.
(19) Aiad, I. A.; Badawi, A. M.; El-Sukkary, M. M.; El-Sawy, A. A.; Adawy, A. I. Synthesis and biocidal activity of some naphthalene-based cationic surfactants. *J. Surfactants Deterg.* **2012**, *15*, 223−234.
(20) Adawy, A. I.; Khowdiary, M. M. Structure and biological behaviors of some metallo cationic surfactants. *J. Surfactants Deterg.* **2013**, *16*, 709−715.
(21) Ibatullina, M. R.; Zhil'tsova, E. P.; Lukashenko, S. S.; Voloshina, A. D.; Sapunova, A. S.; Lenina, O. A.; Nizameev, I. R.; Kutyreva, M. P.; Zakharova, L. Y. Metallomicellar Systems Based on the Complexes of 1-Hexadecyl-4-aza-1-azoniabicyclo[2.2.2]octane Bromide with Transition Metal Nitrates. *Russ. J. Gen. Chem.* **2018**, *88*, 2359−2367.
(22) Zhil'tsova, E. P.; Ibatullina, M. R.; Lukashenko, S. S.; Pashirova, T. N.; Voloshina, A. D.; Zobov, V. V.; Ziganshina, S. A.; Kutyreva, M. P.; Zakharova, L. Y. Complex of 1-hexadecyl-4-aza-1-azoniabicyclo[2.2.2]octane bromide with copper dibromide: structure, aggregation, and biological activity. *Russ. Chem. Bull.* **2016**, *65*, 1365−1371.
(23) Wani, W. A.; Prashar, S.; Shreaz, S.; Gómez-Ruiz, S. Nanostructured materials functionalized with metal complexes: In search of alternatives for administering anticancer metallodrugs. *Coord. Chem. Rev.* **2016**, *312*, 67−98.
(24) Rai, M.; Ingle, A. P.; Medici, S. *Biomedical Applications of Metals*; Springer International Publishing: Cham, 2018.
(25) Romero-Canelón, I.; Sadler, P. J. Next-generation metal anticancer complexes: Multitargeting via redox modulation. *Inorg. Chem.* **2013**, *52*, 12276−12291.
(26) Khowdairy, M.; Badawi, A.; Mohamed, M.; Mohamed, M. Surface and antitumor activity of some novel metal-based cationic surfactants. *J. Cancer Res. Ther.* **2007**, *3*, 198−206.
(27) Kaur, G.; Kumar, S.; Dilbaghi, N.; Bhanjana, G.; Guru, S. K.; Bhushan, S.; Jaglan, S.; Hassan, P. A.; Aswal, V. K. Hybrid surfactants decorated with copper ions: Aggregation behavior, antimicrobial activity and anti-proliferative effect. *Phys. Chem. Chem. Phys.* **2016**, *18*, 23961−23970.
(28) Kaur, G.; Kumar, S.; Kant, R.; Bhanjana, G.; Dilbaghi, N.; Guru, S. K.; Bhushan, S.; Jaglan, S. One-step synthesis of silver metallosurfactant as an efficient antibacterial and anticancer material. *RSC Adv.* **2016**, *6*, 57084−57097.
(29) Veeralakshmi, S.; Nehru, S.; Sabapathi, G.; Arunachalam, S.; Venuvanalingam, P.; Kumar, P.; Anusha, C.; Ravikumar, V. Single and double chain surfactant-cobalt(III) complexes: The impact of hydrophobicity on the interaction with calf thymus DNA, and their biological activities. *RSC Adv.* **2015**, *5*, 31746−31758.
(30) Suganthi Devi, R.; Kumaraguru, N. Ruthenium (II) polypyridyl metallosurfactant complexes: Synthesis, Interaction of CT-DNA and Antitumour study. *Res. J. Pharm. Technol.* **2021**, *14*, 2691−2700.
(31) Jan, R.; Khan, M. S.; Hassan, N.; Mushtaq, U.; Khanday, F. A.; Bhat, M. A. Synthesis, surface activity, self-aggregation and cytotoxicity of ruthenium(II) and Oxovanadium(IV) based metallosurfactants. *J. Mol. Liq.* **2021**, *331*, 115696.
(32) Ambika, S.; Manojkumar, Y.; Arunachalam, S.; Gowdhami, B.; Meenakshi Sundaram, K. K.; Solomon, R. V.; Venuvanalingam, P.; Akbarsha, M. A.; Sundararaman, M. Biomolecular Interaction, Anti-Cancer and Anti-Angiogenic Properties of Cobalt(III) Schiff Base Complexes. *Sci. Rep.* **2019**, *9*, 2721.
(33) Kaur, G.; Kumar, S.; Dilbaghi, N.; Kaur, B.; Kant, R.; Guru, S. K.; Bhushan, S.; Jaglan, S. Evaluation of bishexadecyltrimethyl ammonium palladium tetrachloride based dual functional colloidal carrier as an antimicrobial and anticancer agent. *Dalton Trans.* **2016**, *45*, 6582−6591.
(34) Zhiltsova, E. P.; Ibatullina, M. R.; Lukashenko, S. S.; Valeeva, F. G.; Pashirova, T. N.; Kutyreva, M. P.; Zakharova, L. Y. Complexes of 1-hexadecyl-4-aza-1-azoniabicyclo[2.2.2]octane bromide with transition metal nitrates. Micelle-forming, solubilizing, and adsorption properties. *Colloid J.* **2017**, *79*, 621−629.
(35) Zhiltsova, E. P.; Pashirova, T. N.; Ibatullina, M. R.; Lukashenko, S. S.; Gubaidullin, A. T.; Islamov, D. R.; Kataeva, O. N.; Kutyreva, M. P.; Zakharova, L. Y. A new surfactant-copper(II) complex based on 1,4-diazabicyclo[2.2.2]octane amphiphile. Crystal structure determination, self-assembly and functional activity. *Phys. Chem. Chem. Phys.* **2018**, *20*, 12688−12699.
(36) Zhiltsova, E. P.; Ibatullina, M. R.; Lukashenko, S. S.; Kutyreva, M. P.; Zakharova, L. Y. Spectrophotometric study of quercetin in metallomicellar solutions of 1-hexadecyl-4-aza-1-azoniabicyclo[2.2.2]-octane bromide complex with copper dibromide. *J. Mol. Liq.* **2018**, *249*, 716−722.
(37) Zhil'tsova, E. P.; Ibatullina, M. R.; Lukashenko, S. S.; Kutyreva, M. P.; Zakharova, L. Y. Metallomicellar Complex of 1-Hexadecyl-4-aza-1-azoniabicyclo-[2.2.2]octane Bromide with Copper Dibromide for Solubilization of Nitrofurantoin. *Russ. J. Org. Chem.* **2018**, *54*, 431−435.
(38) Gubaidullin, A. Effect of hydrophilic−hydrophobic ratio in organic molecules on the crystal packing. *Acta Crystallogr., Sect. A: Found. Crystallogr.* **2004**, *60*, s109.
(39) Gubaidullin, A. T.; Beskrovnyj, D. V.; Litvinov, I. A. Crystal structure model based on the analysis of hydrophilic-hydrophobic ratio in molecules. Isosteviol derivatives. *J. Struct. Chem.* **2005**, *46*, S195−S201.
(40) Kitajgorodskij, A. I. *Molecular Crystals and Molecules*; Academic Press: NY, London, 1973.
(41) Kashapov, R.; Razuvayeva, Y.; Ziganshina, A.; Sergeeva, T.; Lukashenko, S.; Sapunova, A.; Voloshina, A.; Kashapova, N.; Nizameev, I.; Salnikov, V.; Ziganshina, S.; Gareev, B.; Zakharova, L. Supraamphiphilic Systems Based on Metallosurfactant and Calix[4]-resorcinol: Self-Assembly and Drug Delivery Potential. *Inorg. Chem.* **2020**, *59*, 18276−18286.
(42) Green, D. R.; Kroemer, G. The pathophysiology of mitochondrial cell death. *Science* **2004**, *305*, 626−629.
(43) Zakharova, L. Y.; Pashirova, T. N.; Kashapov, R. R.; Zhil'tsova, E. P.; Gaisin, N. K.; Gnezdilov, O. I.; Konov, A. B.; Lukashenko, S. S.; Magdeev, I. M. Catalytic properties of micellar systems based on 4-aza-1-alkyl-1-azoniabicyclo[2.2.2]octane bromides. *Kinet. Catal.* **2011**, *52*, 179−185.

https://doi.org/10.1021/acsomega.1c06465
ACS Omega 2022, 7, 3073−3082

(44) Sheldrick, G. M. *SADABS, Program for Empirical X-ray Absorption Correction*; Bruker-Nonius, 2004.
(45) *DIFFRAC Plus Evaluation Package EVA, User's Manual*; Bruker AXS: Karlsruhe, Germany, 2005.
(46) Lisowska, M.; Milczarek, M.; Ciekot, J.; Kutkowska, J.; Hildebrand, W.; Rapak, A.; Miazek, A. An antibody specific for the dog leukocyte antigen DR (DLA-DR) and its novel methotrexate conjugate inhibit the growth of canine B cell lymphoma. *Cancers* **2019**, *11*, 1438.

https://doi.org/10.1021/acsomega.1c06465
ACS Omega 2022, 7, 3073−3082